Experimental testing of a modified active disturbance rejection control for microphonics reduction in a 9-cell TESLA superconducting cavity

A. Elejaga[*] and J. Jugo[†]

Electricity and Electronics Department, University of the Basque Country, Sarriena Auzoa, 48940, Leioa, Spain

P. Echevarria[‡], A. Neumann, and A. Ushakov

Institute of Science and Technology of Accelerating Systems, Helmholtz Zentrum-Berlin, Albert-Einstein-Straße 15, 12489, Berlin, Germany

J. Knobloch

Institute of Science and Technology of Accelerating Systems, Helmholtz Zentrum-Berlin, Albert-Einstein-Straße 15, 12489, Berlin, Germany and Department of Physics, Universität Siegen, 57068, Siegen, Germany

(Received 31 January 2024; accepted 4 November 2024; published 25 November 2024)

This work shows the results obtained with a novel modified active disturbance rejection control (MADRC) algorithm when controlling the detuning of a 9-cell TESLA superconducting radio frequency cavity. This type of control is essential in SRF cavities with high loaded quality factors since they are extremely sensitive to detuning due to their extremely narrow bandwidth. The modification of the active disturbance rejection control is based on loop shaping techniques and confers ease of design and implementation, as well as an improved behavior in presence of delay. To begin with, a theoretical design of the controller based on an experimental transfer function of the cavity is carried out and its performance is compared with that of a proportional integral control. In this preliminary test, the simulation results indicate a remarkable performance superiority of the MADRC. Later, the controller is tested on a TESLA cavity validating both the MADRC algorithm and its design methodology, and achieving a peak detuning reduction of 63%, as well as an rms reduction of 80% with respect to the open loop.

DOI: 10.1103/PhysRevAccelBeams.27.113501

I. INTRODUCTION

Many particle accelerators are immense facilities not only in size and complexity but also in terms of energy consumption. In the current context of climate change and soaring energy prices, current and future facilities need to tackle their efficiency to ensure their viability.

While radio frequency (rf) acceleration has seen significant development over several decades, the evolving demands of future facilities are presenting fresh challenges that are driving advancements in rf acceleration technology. The pursuit of efficient high-gradient rf structures and systems stands as one of the five critical domains identified by the European Strategy for forthcoming facilities [1], needing continued research and development efforts.

Several prominent accelerator facilities worldwide employ high loaded quality factors (Q_L) in low-intensity beam experiments. The high intensity and energy ISOLDE project aims to upgrade the ISOLDE radioactive beam facility at CERN by adding a superconducting linear accelerator (LINAC) among other things. The intended operating point for this accelerator falls within the range of $Q_L = 1 \times 10^7$–3×10^7, with a corresponding cavity bandwidth of 3–10 Hz [2], which makes the subject of microphonics one of the main challenges to overcome. On the other hand, in the case of the Large Hadron-electron collider (LHeC) [3], the possibility of using energy recovery linacs (ERL) such as the one developed in the BERlinPro project is being considered [4] in order to accelerate electrons. For this purpose, a high power energy recovery facility called PERLE has been proposed, in which beam loading is negligible and high Q_L is expected to be used [5]. Another clear example of the necessity of high Q_L operation in low beam-loading applications is the possible upgrade of the European XFEL to continuous

[*]Contact author: ander.elejaga@ehu.eus
[†]Contact author: josu.jugo@ehu.eus
[‡]Contact author: pablo.echevarria@helmholtz-berlin.de

wave (cw) [6]. For this purpose, the cavities are expected to operate with Q_L values between 10^7 and 10^8 and field gradients higher than 16 MV/m.

Cavities that are being operated with such high Q_L are especially susceptible to a phenomenon called microphonic detuning [7], which refers to the detuning caused by mechanical oscillations that couple to the accelerating structures and impact their performance. These mechanical disturbances micrometrically alter the geometry of the cavities, shifting the resonance frequency of the accelerating mode with respect to the nominal frequency. This deformation generates a drift in the phase and amplitude of the electromagnetic field inside the resonator that has traditionally been corrected by the low-level radio frequency (LLRF) control system at the cost of injecting more rf power. Such vibrations can arise from various sources, including ambient acoustic noise, pressure oscillations in the helium system, Lorentz forces, and mechanical resonances in the accelerator components.

In low beam-loading SRF accelerators, controlling the detuning of the resonators allows the reduction of the overcoupling, which is mainly given to manage the expected detuning level of a cavity. Reducing the detuning reliably to an insignificant level will allow to operate cavities at low bandwidth, meaning high loaded quality factor (Q_L). When the quality factors are optimized, the power consumption required to attain a specific level of accelerating field diminishes, resulting in a reduction in rf cost and the possibility of using solid state amplifiers, which are cheaper and more versatile than klystrons. Furthermore, the reduction of microphonics implies an improvement of the field stability which has a direct impact on beam properties.

Active and passive control strategies are used to mitigate microphonics, commonly in conjunction with each other.

Passive control techniques aim to attenuate microphonics through mechanical and structural design strategies without requiring active feedback systems. These methods rely on the inherent properties of the cavity and its support structure to passively mitigate vibrations. Some common passive control techniques include the mechanical isolation of the cavity [8], the stiffening of the structure of the cavity via stiffening rings [9], the addition of materials with high damping properties in critical areas [10], and the attenuation of known vibration sources, such as those generated in the cryogenic system [11].

Active control techniques involve real-time monitoring and correction of microphonics using feedback or feed-forward control systems. These methods aim to actively counteract the vibration-induced disturbances through electromagnetic or mechanical adjustments.

Feed-forward systems are commonly used to correct vibrations whose frequency is fixed and localized, either because they are generated by a constant disturbance or because they are located in one of the mechanical resonance modes of the cavity. In [12], an adaptive feed-forward controller is used to control microphonics derived from mechanical eigenmodes. Another clear example of feed-forward control is the narrowband active noise control (NANC) techniques used in [13], where microphonic detuning produced by rotary machinery, such as vacuum pumps or heating, ventilation and air conditioning systems equipment, is greatly reduced. A similar technique is used in [14], where a modification of the active noise control is applied with an adaptive process based on a least mean square (LMS) algorithm.

In the case of low-frequency stochastic disturbances, like those generated by fluctuations in the liquid helium flow or environmental noise, the use of feedback control systems is necessary. The traditional proportional-integral (PI) controller has been used in various machines [15] and is very effective when the phase response of the tuner is a monotonous function of frequency which is usual at lower frequencies (up to 10 Hz). At higher frequencies, the tuner-cavity system typically has mechanical eigenmodes that introduce steps in the phase response which may possibly lead to positive feedback and instability even at modest gains. This is where the difficulty of controlling this type of system lies. In order to circumvent this problem, arbitrary digital control filters can be optimized specifically to compensate for a given microphonics spectrum while taking into account the exact phase response of the tuner-cavity system [16]. The main disadvantage of this technique is that it is mandatory to exhaustively study the dynamics of the system in order to design the filters, and therefore the system must be recharacterized whenever its response changes.

This paper presents the application of a feedback-based active control solution in which the peak detuning is reduced by active vibration damping using piezoelectric actuators. The selected control algorithm for that matter is the novel modified active disturbance rejection control (MADRC) [17], a modification made to the active disturbance rejection control (ADRC) [18] in order to make it more resilient to delay. The experiment has been carried out at the Helmholtz-Zentrum Berlin (HZB), in which the MADRC algorithm was applied to a 9-cell SRF TESLA cavity with a loaded Q ranging from 6×10^6 to 4×10^7. The obtained detuning reduction is analyzed and discussed to elucidate the validity of the proposed controller.

The basic idea behind ADRC is to estimate and compensate for the disturbance or uncertainty affecting the system in real time by incorporating an extended state observer (ESO) within the control loop. This controller provides robustness, ensuring stability and performance even in the presence of parameter variations and model uncertainties. It is also adaptable to different systems and operating conditions, eliminating the need for accurate mathematical models, and exhibits high perturbance rejection capabilities. It is a simple yet powerful control technique with potential for superior performance.

However, like other control techniques, ADRC control has practical limitations. One significant restraint arises from the presence of time delay, which reduces the stability range of the closed-loop system. Various methods have been proposed to address this issue within ADRC-based schemes. In [18], Han proposed the possibility of designing the ADRC without considering time delay, which sacrifices performance. Another approach involves using a Padé approximation, increasing the system order, but it is only suitable for small time delays [19,20]. To take into account the time delay, it has been suggested in [21,22] to introduce a delay in the control signal before it enters the ESO. In [23], a Smith predictor-based generalized proportional integral control is proposed for input-delayed nonlinear mechanical systems. Castañeda *et al.* [24] propose a predictor scheme for time delay compensation in uncertain time-delay systems. Fu and Tan [20] present a 2 degrees of freedom (2 d.o.f.) control structure for unstable time-delayed systems. More recently, ADRC designs based on probabilistic robustness have been applied to systems with delay [25]. While these methods improve stability in the presence of time delay, they may reduce the disturbance rejection effect.

In the case of the MADRC, the classical ADRC has been rewritten in order to facilitate the stability analysis of the resulting closed loop system, in the presence of time delay. This analysis enables a more detailed frequency domain study and the detection of the frequency range in which the system tends to destabilize. This scheme allows the addition of control elements, designed by loop shaping techniques, which improve the system's relative stability, maintaining the disturbance rejection characteristics of the controller. In summary, the MADRC adds the benefits of the PI controllers, with an easier design strategy for increasing the stability range of the system and thus improving the disturbance reduction. The details of the MADRC algorithm are shown in Sec. II [17].

The paper is organized as follows: In the first section, the structure of the proposed MADRC will be presented in detail and the theoretical and mathematical framework will be developed. Next, the setup used to carry out the experiment will be described, as well as the technical details of the experiment. In a third chapter, the results obtained will be shown and analyzed, ending with a chapter of conclusions in which the validity of the algorithm will be discussed, as well as questions of interest such as future steps or possible improvements.

II. MADRC ALGORITHM

As previously mentioned, the MADRC presented in this paper is a modification of the original ADRC [26], designed to improve the behavior of the controller in the presence of delay. The theoretical basis of this controller is described in depth in [17], so in this section, the algorithm will be presented, emphasizing only the most representative characteristics. The basic composition of the controller is shown in Fig. 1.

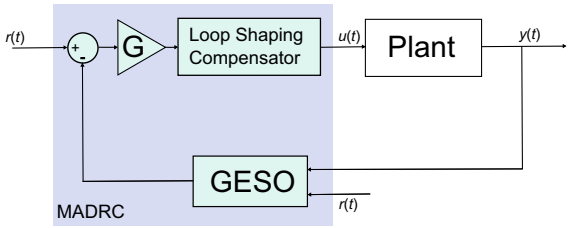

FIG. 1. Structure of the novel MADRC composed of a loop shaping compensator and a generalized ESO. The signals $r(t)$, $u(t)$, and $y(t)$ are the reference signal, the control signal, and the system output, respectively.

The structure of the algorithm has been redefined in order to eliminate feedback from the direct chain, without modifying the position of the controller poles, which are the ones that to a large extent define the dynamics of the system and its stability. In this way, it is easier to analyze the open-loop frequency response of the system, thus locating the frequency ranges in which the closed-loop system has low-relative stability or is directly unstable. Then, by means of the loop shaping compensator, it is possible to modify the amplitude and phase of the system in that problematic frequency range to increase its relative stability. The algorithm has also been redesigned to ensure that the controller always includes an integral action, regardless of the controller gain. It is important to note that modifying the direct loop gain does not result in exactly the desired system dynamics. In other words, the internal disturbance model does not fully match the actual disturbance affecting the system, thus not fulfilling the matching condition, a key principle in ADRC. However, the proposed design methodology is effective in approximating this matching condition as closely as possible while maintaining closed-loop stability.

A. Mathematical description

The working principles of this algorithm are similar to those of the ADRC, so they will not be discussed in this paper, although the most representative differences will be presented. In this way, the GESO can be expressed by its state-space representation as follows.

$$\begin{cases} \dot{\hat{z}}(t) = A_g\hat{z}(t) + B_g\begin{pmatrix} r(t) \\ y(t) \end{pmatrix} \\ y_g(t) = K_0\hat{z}(t) \end{cases}. \tag{1}$$

Being $\hat{z}$ the estimated state space vector, which defines the state of the GESO at any specific point in time. Subsequently, A_g and B_g are defined by the following equations:

$$A_g = A_0 - L_0C_0 - K_0B_0, \tag{2}$$

$$B_g = \begin{pmatrix} B_0 & L_0 \end{pmatrix}. \tag{3}$$

With $p = n - m$ being the relative order of the plant, the matrices A_0, B_0, and C_0 can be defined as follows:

$$A_0 = \begin{pmatrix} 0 & 1 & 0 & \cdots & 0 \\ 0 & 0 & 1 & \cdots & 0 \\ \vdots & \vdots & \vdots & \ddots & \vdots \\ 0 & 0 & 0 & \cdots & 1 \\ 0 & 0 & 0 & \cdots & 0 \end{pmatrix}_{(p+1)x(p+1)}, \tag{4}$$

$$B_0 = (0 \quad \cdots \quad 0 \quad 1 \quad 0)^T_{(p+1)x1}, \tag{5}$$

$$C_0 = (1 \quad 0 \quad 0 \quad \cdots \quad 0)_{(p+1)x1}. \tag{6}$$

$K_0 = (k_1 \quad k_2 \quad \cdots \quad k_p \quad 1)$ is the vector that defines the desired closed-loop dynamic of the controlled system. It can be designed by choosing the controller's bandwidth ω_c and then solving the pole placement problem defined by it. Note that if $p = 1$, then $B = (1\ 0)^T$ and $C = (1\ 0)$.

$L_0 = (l_1 \quad l_2 \quad \cdots \quad l_{p+1})^T$ is another designing parameter that defines the bandwidth of the observer ω_e, thus delimiting the frequency range in which possible disturbances will be corrected. This vector must be selected in such a way that the poles of the ESO are placed in the desired bandwidth and A_g is asymptotically stable. It is important to note that the dynamics of the observer must be several times faster than that of the system.

Figure 2 shows the basic composition of the GESO, which is a generalization of the ESO used in the original ADRC.

One of the most relevant differences with respect to the original ADRC is the addition of the loop shaping compensator. This is a filter used to shape the frequency response of the system in order to improve its relative stability. Different filters may be involved, such as notch filters, lead-lag filters, or proportional, integral, devirative controllers (PIDs), depending on the needs of the system. In addition to that, the MADRC approach allows the frequency response of the feedback loop to be adjusted in a straightforward way while maintaining most of the ADRC formalism. Finally, the integral action is always present in the MADRC algorithm, regardless of the direct loop gain G. This enables the controller to be adjusted by means of this parameter to bring it to its stability limit, maintaining an integral action in the controller.

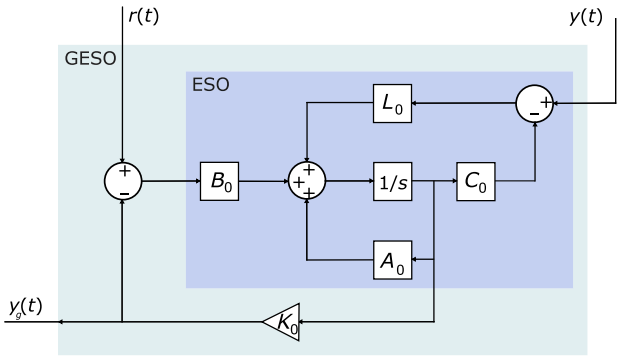

FIG. 2. Representation of the structure of the GESO in which the relation with the original ESO is shown. The signals $r(t)$, $u(t)$, and $y(t)$ are the reference signal, the control signal, and the system output, respectively.

B. Designing methodology

When developing this algorithm, the need for a straightforward process for the controller design, regardless of the system to be controlled, was taken into account. One of the major advantages of the MADRC is that it is not necessary to know the dynamics of the plant, although it is useful when designing the loop shaping compensator. This is very useful for big facilities, as the operator could set the controller parameters without a detailed knowledge of the specific behavior of a given cavity. The method for designing and adjusting the controller is as follows: (1) Select the bandwidth of the observer, ω_e. This parameter determines the frequency range in which the controller acquires information about the disturbances to suppress and is closely related to the stability of the system. As demonstrated in previous work [17], the stability decreases the larger the bandwidth of the observer. This is because at higher frequencies, the effect of the delay in the phase of the system is greater. Thus, the observer bandwidth is set as large as the delay allows. For systems with little relative stability, a conservative approach is to choose the bandwidth a decade larger than the highest frequency disturbance to be rejected. (2) Set the bandwidth of the controller, ω_c. This step determines the final dynamics of the system and therefore varies depending on the application. In any case, it should be at least 10 times smaller than the bandwidth of the observer. (3) Once implemented, it is advisable to start with almost no gain G and gradually increase it until the desired dynamics are fulfilled. If the relative stability of the system is small, either because of the delay or because of its own characteristics, it may destabilize before the desired disturbance rejection and dynamics are achieved. In that case, a loop shaping compensator will be needed. (4) If the plant transfer function is known, the filter can be designed based on frequency domain techniques. If there is no information about the plant, it is possible to gradually increase the gain (G) until the system goes unstable and measure the frequency in which the instability occurs. Then, implement a loop shaping compensator such us a notch filter in order to drastically decrease the action of the controller in that problematic frequency, without affecting the performance in the rest of the bandwidth.

III. CHARACTERIZATION OF THE TUNER-CAVITY SYSTEM

Although it is not strictly necessary to know the dynamics of the system to design the MADRC, it is very

useful when analyzing its viability and studying the effect of its different components. The availability of an approximate transfer function allows the analytical design of the controller, including the loop shaping compensator, to later validate its operation in the real system.

It is important to emphasize that the experimental part of this work takes advantage of the measuring setup, and all the previous studies carried out by Dr. Neumann and colleagues [12].

A. Detuning measurement

The resonance frequency of a cavity is exclusively dependent on its geometry. Thus, when a vibration is coupled to the system, it generates a micro-metrical deformation that causes a drift in its resonance frequency. In TESLA cavities, a change of the cavity length by a mere 1 nm results in a frequency shift of 0.3 Hz, which is especially relevant when operating with high Q_L, due to the extremely narrow bandwidth of the cavity.

When a cavity is fed by a fixed frequency derived from a master oscillator and a detuning event occurs, the cavity responds with a reduction of the field amplitude and a phase shift $\Delta\Phi$. It is possible to relate the detuning Δf to the phase shift by means of the following equation [12].

$$\Delta f(t) = f_0 - f = \frac{f_0}{2Q_L}\tan[\Delta\Phi(t)], \tag{7}$$

where f_0 and f are the fundamental and shifted resonance frequencies respectively. Thus, the phase shift can be used to measure and control the detuning.

The scheme provided in Fig. 3 presents an overview of the rf measurement setup used at HZB's HoBiCaT (Horizontal Bi-Cavity Test facility) [27] for detuning measurements. The cavity operates in an open loop configuration, driven by a tunable master oscillator. The forward wave signal from this source is split to create a signal path for phase error measurement.

In order to feed the cavity, the rf signal is amplified by a solid state amplifier (SSA). By utilizing a three-stub tuner and adjusting the variable penetration depth of the TTF-III input coupler antenna into the beam pipe coupler port, the coupling strength can be varied. This allows for coverage of Q_L ranging from 2×10^8 down to 5×10^6.

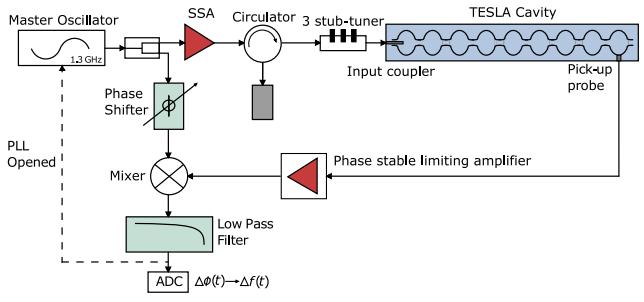

FIG. 3. Standard rf setup at HoBiCaT for continuous wave detuning measurement.

To extract the transmitted power signal and observe the excited rf resonance of the cavity a pickup antenna with a weak coupling strength ($Q_{\text{ext}} \approx 5 \times 10^{11}$) is employed.

For precise phase and detuning measurements, the transmitted power signal undergoes amplification using a phase-stable limiting amplifier to eliminate amplitude variations. This ensures a clean phase shift measurement between the reference signal and the transmitted signal at a low-noise rf mixer. Any phase offsets introduced by the rf cabling can be compensated using a phase shifter in the reference signal path.

The phase error signal is further processed by a low-pass filtering amplifier to optimize the signal-to-noise ratio, eliminate higher-frequency components of the mixing process, and prevent aliasing caused by the subsequent sampling process. Sampling frequencies within the range of 1.0–5.0 kHz are chosen to cover the detuning range of several hundred Hertz.

B. Transfer function measurement

Each accelerating cavity in an accelerator is equipped with a tuning system to adjust the resonance frequency to the desired operating point. In the case of elliptical niobium cavities, stepper motors are utilized along with a lever system to alter the cavity's length. For TESLA cavities, the tuning systems must have a range of approximately 300–500 kHz to compensate for manufacturing tolerances and changes that occur during cooldown.

To compensate for the dynamic Lorentz-force detuning, caused by the pulsed rf mode of operation, modern tuning systems often incorporate an integrated piezo-tuner that helps mitigate such fast detuning events.

In the case of continuous-wave (cw) operated cavities, the pulsed Lorentz-force detuning is not a major concern. However, these fast tuners can still be utilized to compensate for microphonic detuning, which arises from external mechanical vibrations or acoustic disturbances affecting the cavity's resonance.

In this particular case and as it can be seen in Fig. 4, the cavity has a Saclay-II type tuner in which a P-844K075 encapsulated piezo actuator is incorporated [28]. This piezo tuner consists of two piezo-ceramic stacks mounted in a steel sheath.

The setup for measuring the transfer function between the piezo drive signal and the detuning response of the cavity is illustrated in Fig. 5. To ensure precise measurements by excluding the low-pass characteristics resulting from the narrow cavity bandwidth, the loop is closed, operating in a phase-locked-loop configuration. The measurement itself is performed with a lock-in amplifier, which generates the excitation signal while performing low-noise measurements.

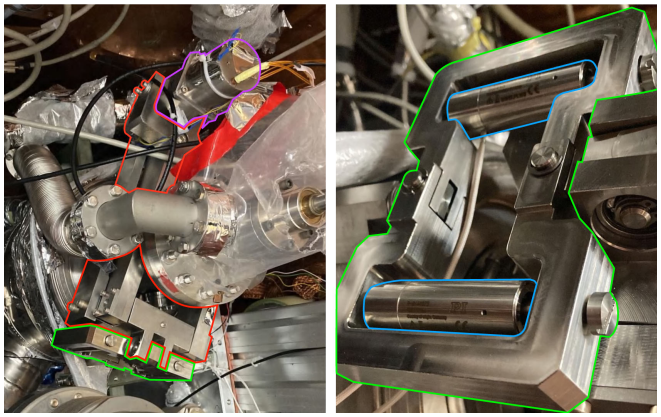

FIG. 4. Saclay tuning system for TESLA cavities. The left picture shows a Saclay-II tuner (red) with a step motor (purple) and a piezo holder (green) mounted on the cryovessel of the cavity. The right picture displays the piezo holder frame (green) designed by HZB with two piezos mounted (blue).

Making use of the piezo-actuator, the system was excited by a sinusoidal signal of variable frequency. A frequency sweep was performed between 0 and 800 Hz, at 0.2 Hz steps. To account for the unknown quality factor of the mechanical modes prior to the measurement, each frequency step was measured for a minimum duration of 2.4 s. This extended measurement time allowed for the acquisition of the steady state response for each data point.

Figure 6 depicts the transfer function that relates the piezo drive signal and the generated detuning in Hz. Given the narrow bandwidth of the cavity in low beam-loading machines, the contribution of eigenmodes above 100 Hz will have limited significance. However, it is important to note that they are relevant in terms of system stability. In fact, the resonance mode at 160 Hz generates an abrupt jump in the phase of the system making its phase margin barely 2°. This means that the system's closed-loop relative stability is extremely low. In addition, above that frequency, the phase continues to deteriorate, which makes it difficult to control this system by means of a feedback controller, at least in that frequency range.

Looking at the phase of the system at low frequencies, where the effect of resonances is not yet apparent, it is possible to observe a linear decay of the phase as the frequency increases. By calculating the group delay (τ_g) in that area, which is defined as the derivative of the phase with respect to frequency ($\tau_g = -\frac{d\phi}{df}$), it is possible to infer that the system delay is approximately 0.12 ms. This stems mostly from the intrinsic delay of the piezoelectric actuator and mechanical tuner.

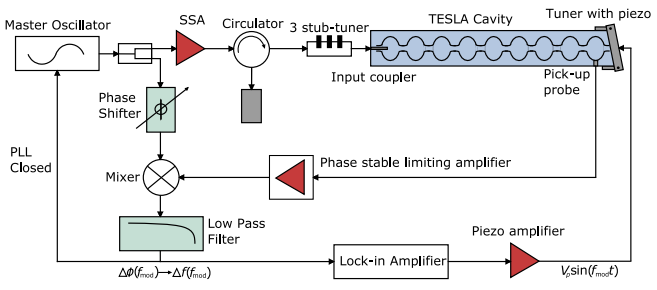

FIG. 5. Measurement setup to obtain the transfer function between piezo excitation and cavity detuning response.

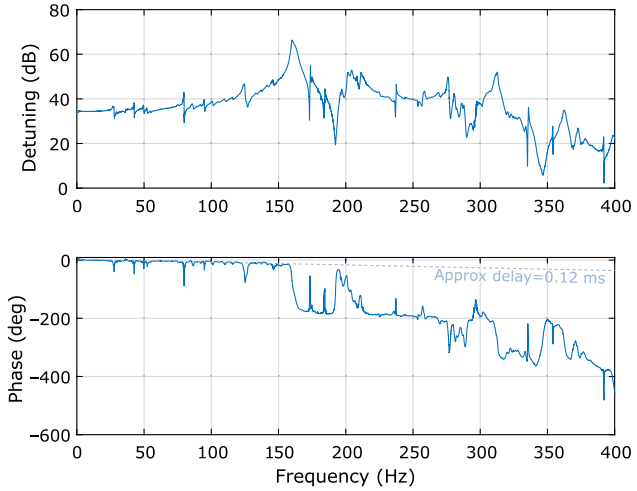

FIG. 6. Bode diagram of the transfer function that relates the piezo drive signal with the detuning, for the system composed by the Saclay-II tuner and the TESLA cavity.

IV. DETUNING CONTROL

As previously mentioned, due to the mechanical characteristics of the cavities, feedback controllers tend to destabilize these systems even at very low gains, obtaining effective bandwidths of a few Hertz. The objective of this controller implementation is to reduce the detuning caused by stochastic effects over the widest possible bandwidth, demonstrate the feasibility of the MADRC algorithm, and discuss its advantages over more traditional controls such as the PID.

A. Theoretical analysis and design

Since a transfer function of the system is available, it is possible to perform a theoretical analysis and design of the controller using tools such as the Bode and Nyquist diagrams. In addition, this allows to compare the expected theoretical behavior and the real one, to ensure unequivocally the feasibility of the design method and the MADRC algorithm.

Due to the relatively large system delay, it will be necessary to find a compromise between disturbance suppression and system stability in the closed loop. Figure 7 depicts the frequency response of a second order MADRC algorithm as a function of the bandwidth of the controller f_c.

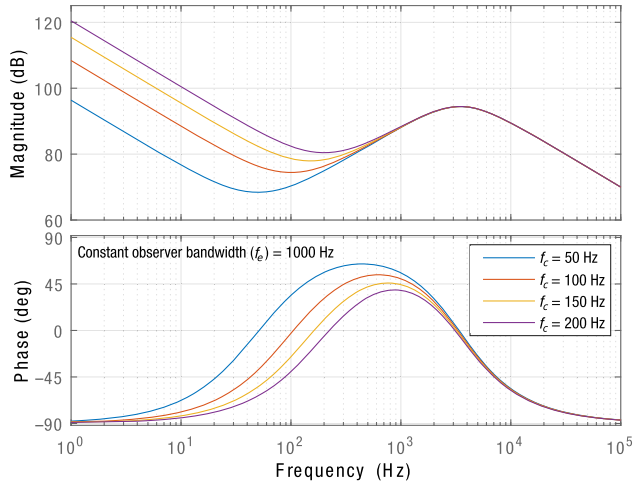

FIG. 7. Bode diagram of a second order MADRC algorithm as a function of the bandwidth of the controller f_c.

The more the bandwidth of the controller is increased, the more the system gain increases at low frequencies, indicating an improvement in disturbance rejection in that frequency range. As far as the phase is concerned, it is possible to observe how the phase increment decreases the higher f_c is. Considering the transfer function shown in Fig. 6, the objective for stabilizing the closed-loop system is to improve the phase in the 160–190 Hz range, so the higher the phase increment of the controller, the more stability it will bring to the system. In conclusion, detuning suppression capabilities increase with the controller bandwidth (f_c), but the stability it brings to the system decreases.

Repeating the same process with the observer bandwidth (f_e) and as shown in Fig. 8, the controller gain increases the larger f_e is, although it should be noted that the effect is greater at higher frequencies. This means that in the case of a system with delay, the bandwidth of the observer can negatively influence the stability of the system, since for the system to be stable, it is necessary that the gain of the controlled system is less than 0 dB above the phase crossover frequency, which decreases due to time delay. As far as phase is concerned, it also improves the wider the bandwidth, so in theory, for a nondelayed system, the performance of the controller is higher the wider the bandwidth of the observer. In this particular case, as the system has a relatively large delay, the bandwidth of the observer is limited by the stability of the system, since it is not desirable for the system gain to be large at high frequencies. In addition, the phase distortion arising from the discretization when the observer dynamics is too fast is also detrimental to the stability of the system. It should also be taken into account that the higher the bandwidth f_e, the higher the execution speed of the controller, and consequently, the higher the needed computational power of the hardware used.

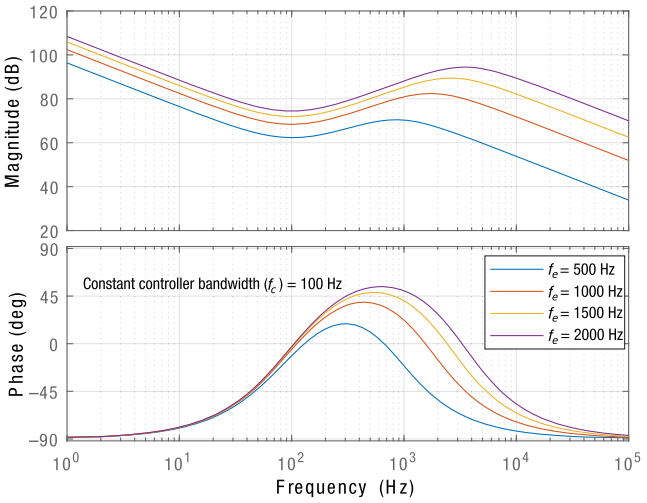

FIG. 8. Bode diagram of a second order MADRC algorithm as a function of the bandwidth of the observer f_e.

In any case, the phase lead shown in Figs. 7 and 8 introduced by the controller increases the relative stability of the system, being this one of the interesting characteristics of such controller.

It is also worth mentioning that the gains shown in both Figs. 7 and 8 are that high due to the very nature of the MADRC. Ideally, this algorithm is designed to suppress any dynamics that differ from those desired for the system, resulting in a notably high open-loop gain over most of the bandwidth and especially at low frequencies. However, it should be remembered that the controllers shown in these figures are ideal, although they clearly represent the loop shaping introduced by this kind of elements. In practice, it is necessary to adjust the gain of the MADRC via the control variable G (see Fig. 2) so that the system is not destabilized.

Based on the above and through trial and error, it is determined that a second order MADRC with bandwidths of $f_c = 170$ Hz and $f_e = 2000$ Hz is appropriate for this particular system. To adjust the controller, the gain G is gradually increased, starting from zero, until the best disturbance rejection performance is achieved. This information is obtained from the magnitude of the bode diagram of the closed-loop system. It should be noted that as the gain increases, the stability of the system decreases until destabilization is reached. Thus, it is important to reach a compromise between performance and relative stability. To analyze the stability of the system, it is possible to study the Nyquist diagram of the open-loop system. By following this process, a gain of $G = 3.62 \times 10^{-6}$ is obtained.

At this point, the objective is to improve the relative stability of the system in order to further increase the gain and achieve a better suppression of disturbances as well as a wider bandwidth. This can be done by implementing a large range of filters as a loop shaping compensator device. By analyzing the frequency response of the open loop

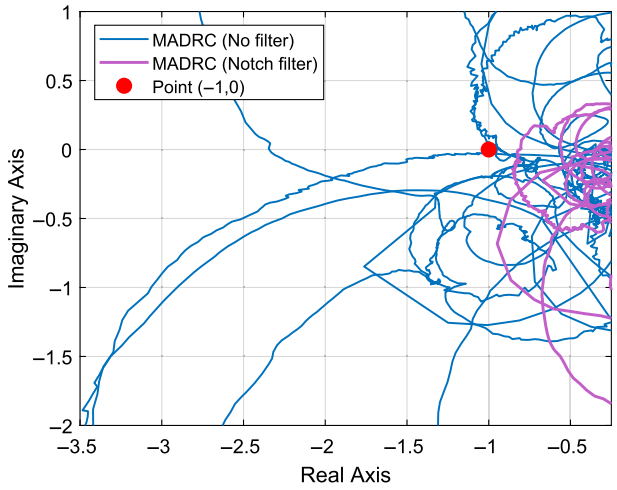

FIG. 9. Simulated Nyquist diagram of the system with and without loop shaping compensator obtained using the measured cavity's frequency response. The gain of the controller for both cases is 7.5×10^{-6}.

system when the instability occurs, it is determined that the instability is generated at around 170 Hz as could already be predicted by observing the transfer function shown in Fig. 6. Thus, an auxiliary controller $C(s)$ has been designed in order to modify the loop shape. In this particular case, a notch filter centered at 170 Hz is implemented in order to decrease the gain of the controller in that particular frequency and stabilize the system.

Looking at the Nyquist diagram [29] of the open loop system shown in Fig. 9, it can be seen that in the unstabilized system (blue line), there is a resonance surrounding the point $(-1, 0)$, which is the one located at 170 Hz. After applying the notch filter and stabilizing the system, it can be noticed how the circumference that represents that resonance decreases to the point of not surrounding the point $(-1, 0)$ anymore. This filter is defined by Eq. (8) and its effect can be seen in the Nyquist diagram in Fig. 9.

$$C(s) = \frac{s^2 + 1140926}{s^2 + 854s + 1140926}. \tag{8}$$

Once the system is stabilized, it is possible to further increase the gain ($G = 9.1 \times 10^{-6}$) of the controller to improve its performance. Figure 10 shows the closed-loop frequency response of the system for the MADRC with and without loop shaping compensator. It is also shown the system response with a well-tuned proportional (P) and proportional-integral (PI) controller.

It should be recalled that all this process is carried out through computational methods using the model obtained in Sec. III B, so the results shown are the product of a computational simulation.

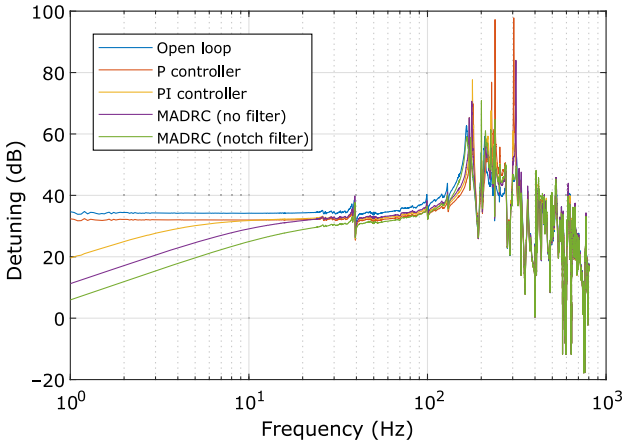

FIG. 10. Simulated frequency response of the closed-loop system for different controllers, obtained using the measured frequency response of the cavity.

Comparing the MADRC with the PI, the former offers greater detuning reduction over a wider bandwidth, approximately 30 Hz. It is also demonstrated that with the appropriate loop shaping compensator, a notch filter in this case, it is possible to improve the performance of the controller by making it more stable and thus increasing its gain.

B. Control setup

As far as the control setup is concerned, the same measurement method described in the previous chapter is used. In this case, the loop is closed by the mechanical control, so the master oscillator operates with the PLL loop opened and generating a constant driving signal of 1.3 GHz. The signal that is fed into the controller as a reference is the phase difference obtained by comparing the incident and transferred signal. Thus, technically, a phase control is performed, although the direct relationship between detuning and phase shift can be observed in Eq. (7). The control signal is amplified before driving the piezo tuner, as it is depicted in Fig. 11.

The implementation is done on the FPGA of a FlexRIO NI-7935R, so there is enough execution speed to set the observer bandwidth high enough to experiment with different controller configurations. In this way, the controller is

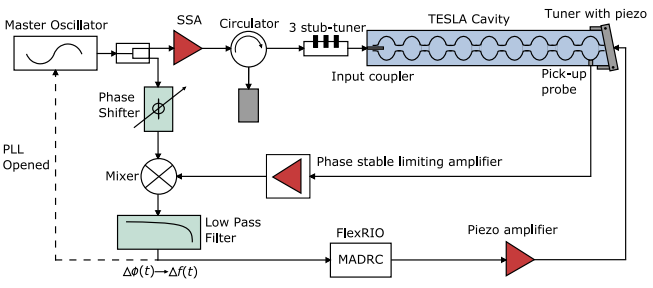

FIG. 11. Control setup used in HZB to compensate for detuning of a TESLA cavity.

implemented with an execution rate of 10 MHz. In addition, an NI-5783 IO module is used, which provides an acquisition or generation speed of 100 MHz and a full-scale output range of 2 V peak to peak. Considering that the piezo amplifier has a gain of 20, the dynamic range of the control signal is ±20 V, which constitutes 20% of the operational range of the piezo tuner. It is worth mentioning that the implementation of the controller was previously tested and debugged using the virtual SRF cavity developed as a result of the collaboration between HZB and the University of the Basque Country [30].

C. Experimental results

For this experiment, the input coupler and the three stub tuner were arranged so that the Q_L of the cavity was fixed at 10^7. The cavity was fed by a 400 W driving signal generating a field gradient of 4 MV/m. No amplitude or phase control of the rf signal was used in this experiment. Then, by means of one of the piezo tuners, a frequency constant mechanical disturbance of 11.4 Hz was introduced in order to replicate possible perturbations that the cavity may suffer during its real operation and to have a known disturbance on which to measure the reduction obtained by our controller.

Following the design method described in Sec. II B, we first determined the bandwidths of both the observer and the controller. Taking as a starting point the values obtained in the theoretical section and taking into account the possible discrepancies between the measured transfer function (Fig. 6) and the real system, we proceed to test different MADRCs to find the optimal controller to which we will later apply the loop shaping compensator. The bandwidth of the observer was fixed at 2000 Hz, and we experimented with different controller bandwidths obtaining the results shown in Fig. 12. The gain of all

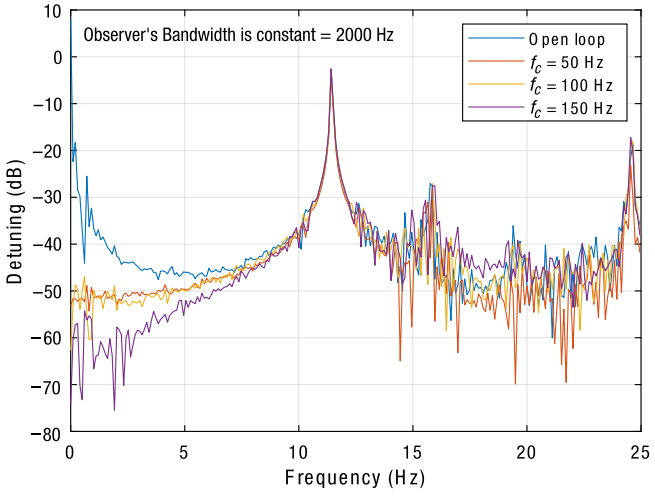

FIG. 12. Frequency spectrum of the measured detuning of the TESLA cavity by using different controller bandwidths. A constant perturbation of 11.4 Hz is being fed into the system.

TABLE I. Measured detuning and bandwidth for different controllers.

	Gain (10^{-4})	rms (Hz)	Bandwidth (Hz)
Open loop	⋯	2.2857	⋯
$\omega_c = 50$ Hz	8.866	0.9005	5
$\omega_c = 100$ Hz	1.067	1.0699	5
$\omega_c = 150$ Hz	0.605	1.0628	7

controllers was adjusted to provide the greatest reduction of disturbances while ensuring system stability. Table I shows the most relevant parameters results for each controller.

As can be seen from both Fig. 12 and the results in Table I, all three controllers have very low bandwidth since the gain is very limited by the stability of the system. Even so, they are able to control the static detuning and reduce the dynamic detuning in a bandwidth of around 5 Hz. In this case, the bandwidth is defined as the frequency range in which the controller is able to reduce the detuning by 3 dB with respect to the open loop.

Note that the gains differ from the limits obtained in the theoretical analysis performed using experimental data. This is attributed to the fact that the system was not under the same electromagnetic conditions on the day the data were taken to perform the mathematical computations and the day the experiment was performed. Even so, the qualitative results are similar.

The next step, which consists of stabilizing the controller by loop shaping, is performed with the controller with $\omega_c = 150$, since it is the one that best reduces disturbances at low frequencies and has the widest effective bandwidth. Thus, following the methodology described in Sec. II B, the controller gain is increased until the system destabilizes. This happens with a $G = 6.6 \times 10^{-4}$ generating an oscillation of 164 Hz, which is very similar to what was predicted in the theoretical analysis. In order to stabilize the system, a notch filter centered at 164 Hz is implemented as a loop shaping compensator, so the gain of the controller in that frequency is drastically decreased maintaining the performance in the rest of the bandwidth. The notch filter is represented by Eq. (9).

$$C(s) = \frac{s^2 + 1061811}{s^2 + 1030s + 1061811}. \tag{9}$$

Once the system was stabilized, we were able to further increase the controller gain to a value of 77×10^{-4}, more than an order of magnitude higher. Figure 13 shows the Bode diagram of the best performing controllers with and without loop shaping compensation. As emphasized earlier, the increase in controller gain G and the associated improvements in performance are made possible by the enhancement of the relative stability of the system obtained by the notch filter.

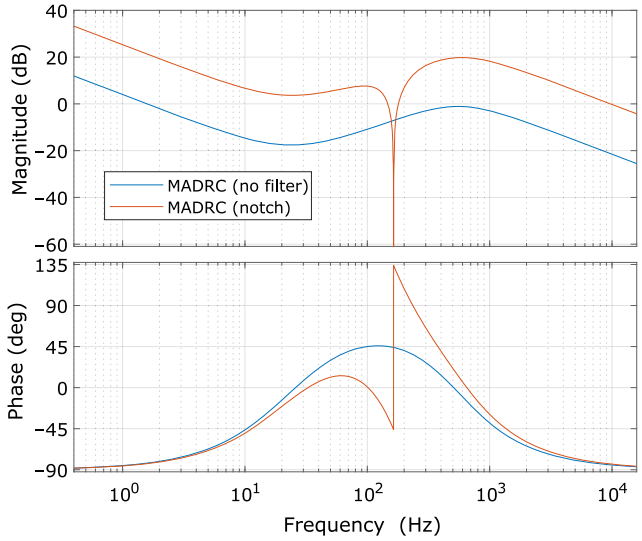

FIG. 13. Bode diagram of the implemented MADRC controller with parameters $\omega_e = 2000$ Hz and $\omega_c = 150$ Hz. The blue plot depicts the dynamics of the MADRC with no loop shaping compensator ($G = 6.6 \times 10^{-4}$). The red plot represents the dynamics of the MADRC in conjunction with the notch filter ($G = 77 \times 10^{-4}$).

This resulted in a bandwidth of approximately 30 Hz, 25 Hz more than what was achieved without loop shaping. In addition, the fixed 11.4 Hz resonance was reduced by 11 dB, which in linear is equivalent to a factor of 4. Figure 14 shows the detuning measured for different controller gains and Fig. 15 illustrates in more detail the reduction achieved on the disturbance generated by the secondary piezo tuner at 11.4 Hz.

In order to better appreciate the bandwidth of the controller and the effect it has on the different mechanical

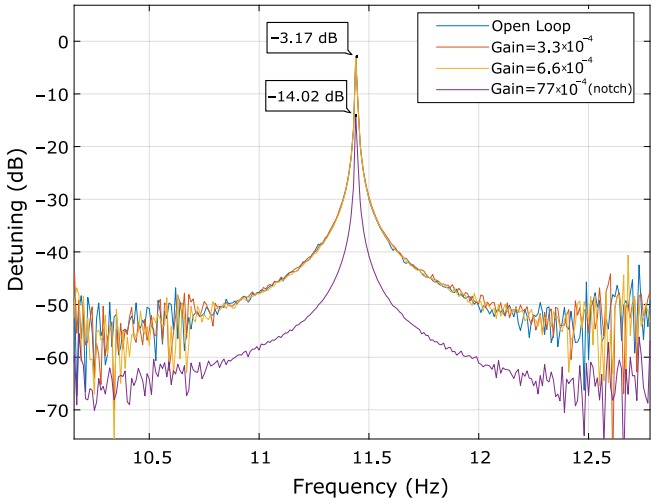

FIG. 15. Close-up of the measured detuning of the TESLA cavity for different controller gains. The parameters of the controller are $\omega_e = 2000$ Hz and $\omega_c = 150$ Hz. A constant perturbation of 11.4 Hz is being fed into the system.

resonance modes of the cavity, Fig. 16 shows the integrated detuning spectra.

Note that the bandwidth and performance of the controller increases with gain. The same conclusions are obtained if we represent the data on a time scale. Figure 17 clearly illustrates the dc correction and the reduction in detuning rms as the gain increases. Table II shows the most representative results for this controller.

It should be emphasized that one of the most important features of the achieved MADRC controller is its broadband microphonic detuning rejection. Table III shows the rms reduction obtained by the different controllers in three

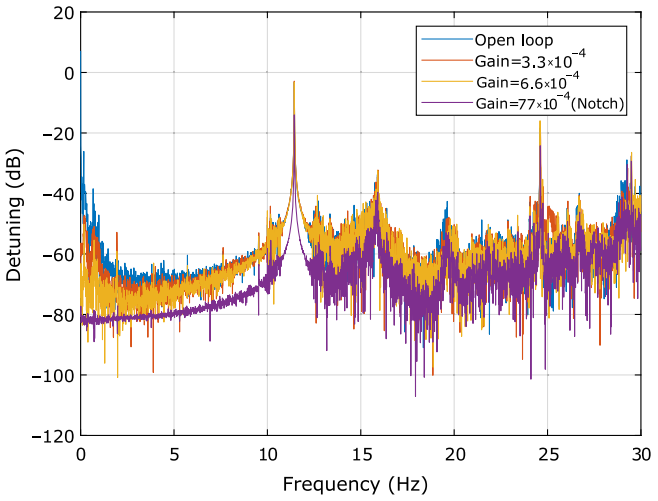

FIG. 14. Frequency spectrum of the measured detuning of the TESLA cavity for different controller gains. The parameters of the controller are $\omega_e = 2000$ Hz and $\omega_c = 150$ Hz. A constant perturbation of 11.4 Hz is being fed into the system.

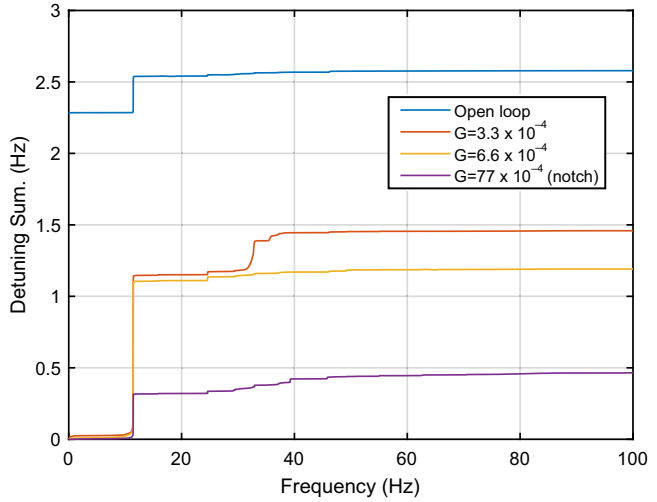

FIG. 16. Integrated detuning frequency spectra of the TESLA cavity for different controller gains. The parameters of the controller are $\omega_e = 2000$ Hz and $\omega_c = 150$ Hz. A constant perturbation of 11.4 Hz is being fed into the system.

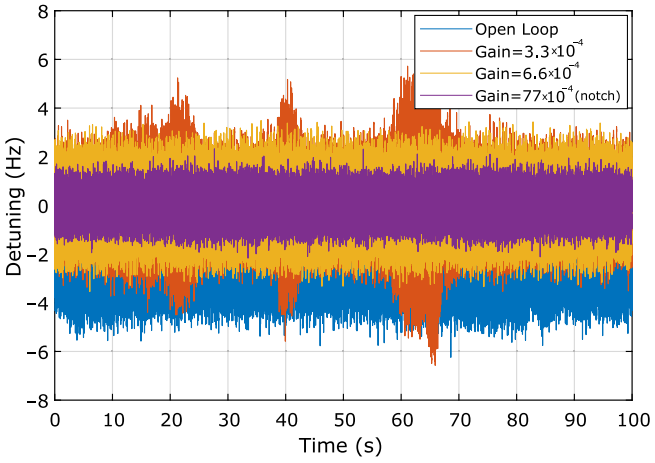

FIG. 17. Measured detuning over time of the TESLA cavity for different controller gains. The parameters of the controller are $\omega_e = 2000$ Hz and $\omega_c = 150$ Hz. A constant perturbation of 11.4 Hz is being fed into the system.

different frequency bands; the frequencies before the 11.4 Hz constant disturbance, the frequencies after, and the rms reduction specifically related to that disturbance. As it can be seen in such table, the reduction of microphonics is relatively constant over the whole bandwidth, not only reducing the artificially introduced perturbation, but any disturbance within the bandwidth of the controller.

Thus, the feasibility of the MADRC algorithm and the proposed design method is evident. As shown in Table II, the MADRC adjusted by loop shaping techniques is able to reduce the detuning (rms) by a factor of 5 with respect to the open loop. Furthermore, it is evident that the controller's performance is significantly reduced when the stabilization step by loop shaping is absent. This is due to the lower relative stability, which prohibits increasing the gain without destabilizing the system, leading to a performance degradation of more than 60%. It is worth mentioning that experiments have been performed with different values of Q_L and disturbance frequencies, varying from 10^7 to 5×10^7 and from 5 to 20 Hz, respectively, and the result has been very similar.

TABLE II. Measured detuning and bandwidth for different gains with the same controller ($\omega_e = 2000$ Hz and $\omega_c = 150$ Hz).

Gain (10^{-4})	Peak value (Hz)	rms (Hz)	Bandwidth (Hz)
Open loop	6.2424	2.5877	...
3.3	7.2179	1.4824	3
6.6	3.5389	1.2264	7
77	2.3252	0.5297	29

TABLE III. Measured rms detuning for different gains of the controller ($\omega_e = 2000$ Hz and $\omega_c = 150$ Hz) in four different frequency ranges.

Gain	rms (Hz) 0–11.4 Hz	rms (Hz) 11.4 Hz	rms (Hz) 11.4–29 Hz	rms (Hz) 29–100 Hz
Open loop	2.2879	1.0950	0.2704	0.3781
3.3	0.1710	1.1317	0.2585	0.4908
6.6	0.1191	1.0931	0.2904	0.3555
77	0.0350	0.3137	0.1234	0.3188

V. SUMMARY AND CONCLUSION

Based on the measured transfer function, a well-tuned MADRC was designed and proven in simulation in Sec. IV A. On the one hand, it was shown that the MADRC algorithm in itself offers better performance than the most commonly used PI, since it offers greater reduction of disturbances in a wider bandwidth (see Fig. 10). The feasibility of the stabilization system based on loop shaping was also demonstrated. By providing the system with greater relative stability through the implementation of filters, it has been possible to increase the gain of the controller, increasing at the same time its performance and bandwidth.

In Sec. IV C, both the MADRC algorithm and the design methodology were experimentally validated. For that matter, a 9-cell TESLA cavity equipped with a Saclay-II tuner was used, which is located in the HoBiCaT test bench at the Helmholtz-Zentrum Berlin. Through trial and error, it was determined that the optimum parameters for the controller were $\omega_c = 150$ Hz and $\omega_e = 2000$ Hz, which is in agreement with the results obtained in simulation. The relationship between the controller gain and its performance was also demonstrated, since as shown in Fig. 14, the higher the gain parameter, the greater the bandwidth and detuning reduction. Finally, the validity of our stabilization method using loop shaping was demonstrated. By implementing a notch filter centered at 164 Hz, not only were the simulation results matched, but they were significantly improved. An rms of 0.5 Hz was achieved, 50% lower than that obtained in the simulation, along with a bandwidth of 29 Hz.

From all this, although more analysis is needed for a deeper understanding of the overall system performance, we conclude that the MADRC algorithm is a strong candidate for the control of low frequency stochastic microphonics. It is easy to implement and design and does not require too much prior information about the system to be controlled. In that sense, it shares many of the benefits and strengths of classical PID controllers but with better overall performance.

Compared to the classic ADRC, the alternative MADRC structure offers two important advantages. On the one hand, it allows to analyze the open-loop frequency response more easily, facilitating the stabilization process. On the other hand, it is designed in such way that the matching condition

is always met regardless of the controller gain. This allows the gain to be used to bring the system to its stability limit, which later allows a stabilization filter to be designed with relative ease.

Finally, it should be noted that this is a feedback controller with the objective of controlling low-frequency stochastic microphonics such as those derived from the pressure fluctuations of liquid helium. Thus, it can be combined with feed-forward control systems to control constant frequency microphonics.

ACKNOWLEDGMENTS

The authors would like to thank S. Klauke, H. Plötz, M. Schuster, and A. Frahm for installing and preparing the experimental setup. We also would like to thank the Basque government, the IT1533-22 grant and the LINAC KK-2024/00065 Elkartek project for financing the Ph.D. and the internship that have made possible to carry out this research.

[1] C. Adolphsen, D. Angal-Kalinin, T. Arndt, M. Arnold, R. Assmann, B. Auchmann, K. Aulenbacher, A. Ballarino, B. Baudouy, P. Baudrenghien *et al.*, European strategy for particle physics–accelerator R&D roadmap, arXiv:2201.07895.

[2] Y. Kadi, M. Fraser, and A. Papageorgiou-Koufidou, HIE-ISOLDE: Technical design report for the energy upgrade, CERN Yellow Reports: Monographs, CERN, 2018.

[3] B. Holzer, M. Klein, O. Brüning, A. Bogacz, and K. André, Accelerator challenges of the LHeC project, in *Proceedings of the 12th International Particle Accelerator Conference(IPAC2021), Campinas, SP, Brazil* (JACoW Publishing, Geneva, Switzerland, 2021), pp. 2570–2573.

[4] M. Abo-Bakr, W. Anders, A. Büchel, K. Bürkmann-Gehrlein, A. Bundels, Y. Bergmann, P. Echevarria, A. Frahm, H.-W. Glock, F. Glöckner *et al.*, Status report of the Berlin energy recovery linac project BERLinPro, in *Proceedings of the 9th International Particle Accelerator Conference (IPAC 2018), Busan, Korea* (JACoW Publishing, Geneva, Switzerland, 2018), pp. 4127–4130.

[5] M. Klein and A. Stocchi, PERLE: A high power energy recovery facility for Europe A Contribution to the Update of the European Strategy on Particle Physics, Technical Report No. CERN LHeC-Note-003-2018, 2018.

[6] A. Bellandi, V. Ayvazyan, J. Branlard, C. Gümüs, S. Pfeiffer, K. Przygoda, and R. Rybaniec, LLRF R&D towards CW operation of the European XFEL, in *Proceedings of the 29th Linear Accelerator Conference (LINAC2018), Beijing, China* (JACoW Publishing, Geneva, Switzerland, 2018), pp. 223–226.

[7] J. Ma, G. Huang *et al.*, Microphonics simulation and parameters design of the SRF cavities for CiADS, in *Proceedings of the 10th International Particle Accelerator Conference, IPAC-2019, Melbourne, Australia, 2019* (JACoW Publishing, Geneva, Switzerland, 2019), pp. 2903–2905.

[8] J. Holzbauer, B. Chase, J. Einstein-Curtis, B. Hansen, E. Harms, J. Kaluzny, A. Klebaner, M. McGee, Y. Orlov, T. Peterson *et al.*, Passive microphonics mitigation during LCLS-II cryomodule testing at Fermilab, Fermi National Accelerator Laboratory (FNAL), Batavia, Technical Report No. FERMILAB-CONF-18-761-AD-TD; 1697794, **2018**.

[9] E. Zaplatin, A. Kanareykin, and V. Yakovlev, Microphonics passive damping, Fermi National Accelerator Lab. (FNAL), Batavia, IL, Technical Report No. FERMILAB-CONF-17-673-TD; 1669443, 2018.

[10] T. Powers, Control of microphonics for narrow control bandwidth cavities, in *Talk Presented at the 2017 International Conference on RF Superconductivity, Lanzhou, China* (2017).

[11] D. K. Ravikumar, Y. R. Than, and J. P. Longtin, Eliminating flow-induced microphonics in a superfluid helium cryogenic system, Cryogenics **104**, 102984 (2019).

[12] A. Neumann, W. Anders, O. Kugeler, and J. Knobloch, Analysis and active compensation of microphonics in continuous wave narrow-bandwidth superconducting cavities, Phys. Rev. ST Accel. Beams **13**, 8, 082001 (2010)

[13] A. Bellandi, J. Branlard, J. D. Cruz, S. Aderhold, A. Benwell, A. Brachmann, S. Hoobler, A. Ratti, D. Gonnella, J. Nelson *et al.*, Narrow bandwidth active noise control for microphonics rejection in superconducting cavities at LCLS-II, arXiv:2209.13896.

[14] N. Banerjee, G. Hoffstaetter, M. Liepe, P. Quigley, and Z. Zhou, Active suppression of microphonics detuning in high Q_L cavities, Phys. Rev. Accel. Beams **22**, 052002 (2019).

[15] Z. Conway and M. Liepe, Fast piezoelectric actuator control of microphonics in the cw cornell ERL injector cryomodule, in *Proceedings of the Particle Accelerator Conference (PAC'09), Vancouver, BC, Canada* (JACoW Publishing, Geneva, Switzerland, 2009), p. 918.

[16] J. Holzbauer, B. Chase, L. Doolittle, J. Einstein-Curtis, Y. Pischalnikov, W. Schappert, and C. Serrano, Active microphonics compensation for LCLS-II, Fermi National Accelerator Laboratory (FNAL), Batavia, IL, Technical Report No. FERMILAB-CONF-18-612-AD-TD; 1697799, 2018.

[17] J. Jugo, A. Elejaga, and P. Echevarria, Modified active disturbance rejection control scheme for systems with time delay, IET Control Theory Appl. **17**, 1992 (2023).

[18] J. Han, From PID to active disturbance rejection control, IEEE Trans. Ind. Electron. **56**, 900 (2009).

[19] W. Tan and C. Fu, Analysis of active disturbance rejection control for processes with time delay, in *Proceedings of the American Control Conference (ACC), 2015* (IEEE, New York, 2015), pp. 3962–3967.

[20] C. Fu and W. Tan, Control of unstable processes with time delays via ADRC, ISA Trans. **71**, 530 (2017).

[21] S. Zhao and Z. Gao, Modified active disturbance rejection control for time-delay systems, ISA Trans. **53**, 882 (2014).

[22] Q. Zheng and Z. Gao, On active disturbance rejection for systems with input time-delays and unknown dynamics, in *American Control Conference (ACC) 2016* (IEEE, New York, 2016), pp. 95–100.

[23] M. Ramirez-Neria, H. Sira-Ramírez, A. Luviano-Juarez, and A. Rodríguez-Angeles, Smith predictor based

generalized PI control for a class of input delayed nonlinear mechanical systems, in *European Control Conference (ECC), 2013* (IEEE, New York, 2013), pp. 1292–1297.

[24] L. Castañeda, A. Luviano-Juárez, G. Ochoa-Ortega, and I. Chairez, Tracking control of uncertain time delay systems: An ADRC approach, Control Eng. Practice **78**, 97 (2018).

[25] Z. Wu, D. Li, and Y. Chen, Active disturbance rejection control design based on probabilistic robustness for uncertain systems, Ind. Eng. Chem. Res. **59**, 18070 (2020).

[26] G. Herbst, A simulative study on active disturbance rejection control (ADRC) as a control tool for practitioners, Electronics **2**, 246 (2013).

[27] J. Knobloch, W. Anders, D. Pflückhahn, M. Schuster *et al.*, Hobicat: A test facility for superconducting rf systems, in *Proceedings of 2003 Workshop on RF Superconductivity, Lübeck/Travemünder, Germany* (JACoW Publishing, Geneva, Switzerland, 2003).

[28] Y. Pischalnikov and C. Contreras-Martinez, Review of the application piezoelectric actuators for SRF cavity tuners, arXiv:2305.06868.

[29] M. Smith, On the generalized nyquist stability criterion, Int. J. Control **34**, 885 (1981).

[30] P. Echevarria, E. Aldekoa, J. Jugo, A. Neumann, A. Ushakov, and J. Knobloch, Superconducting radio-frequency virtual cavity for control algorithms debugging, Rev. Sci. Instrum. **89**, 084706 (2018).